# Breaking of time-reversal symmetry for a particle in a parabolic potential that is subjected to Lévy noise: Theory and an application to solar flare data

Steven Yuvan[1] and Martin Bier[1,2]

[1]*Department of Physics, East Carolina University, Greenville, North Carolina 27858, USA*

[2]*Faculty of Mechanical Engineering and Institute of Mathematics and Physics, University of Technology and Life Sciences, 85-796 Bydgoszcz, Poland*

(Received 30 November 2020; revised 6 April 2021; accepted 14 June 2021; published 15 July 2021)

The noise in nonequilibrium systems commonly contains more outliers as compared to equilibrium systems and is often best described with a Lévy distribution. Many systems in which there are fluctuations around a steady-state throughput can be modeled as a Lévy-noise-subjected particle in a parabolic potential. We consider an overdamped particle in a parabolic potential that is subjected to noise. Microscopic reversibility and time-reversal symmetry apply if the particle is subject to Gaussian distributed noise, but are violated if the noise is Lévy. A parameter to detect this violation is formulated. We, furthermore, develop an understanding for how the time-reversal asymmetry depends on the time $\Delta t$ between the sample points and on the stability index, $\alpha$, of the Lévy noise. With solar flare data it is shown how the time-reversal asymmetry parameter of a signal can be used to obtain the $\alpha$ of the underlying noise.

DOI: 10.1103/PhysRevE.104.014119

## I. INTRODUCTION

For a system to be at equilibrium, there should be no identifiable arrow of time. In other words, when a movie is made of the system, it should afterwards not be possible to determine whether the movie is played forward or backward. In the 1930s Onsager gave mathematical rigor to the idea when he conceived the notion of microscopic reversibility [1,2]. Microscopic reversibility occurs when every trajectory in the state space is traversed equally often in both directions and it is the defining characteristic of equilibrium.

Below we will consider the following Langevin equation:

$$\dot{x} = -\frac{dV(x)}{dx} + \xi_\alpha(t). \tag{1}$$

This equation describes the overdamped motion of a noisy particle in a potential $V(x)$. The coefficient of friction and the amplitude of the noise term $\xi_\alpha(t)$ have been absorbed in the timescale and length scale. The meaning of the subscript $\alpha$ will be explained below.

The function $\xi_\alpha(t)$ represents the noise. In many contexts such noise is the result of collisions of the particle with the molecules of a fluid medium. The term $\xi_\alpha(t)$ thus describes subsequent "kicks" that the particle is subjected to. In 1953 Onsager and Machlup showed how, for a certain class of trajectories, microscopic reversibility ensues when the amplitudes of these kicks have a Gaussian distribution [3–5]. Such a result makes sense in the light of the central limit theorem. This theorem states that if the outcome of a process is the combined result of $N$ independent stochastic processes, then in the limit of $N \to \infty$ these outcomes have a Gaussian distribution [6]. The Gaussian distribution can thus be considered an attractor as $N$ gets larger. The net displacement of a particle in a fluid medium is the result of Brownian collisions and over a timescale that is much larger than the time between subsequent collisions that net displacement is expected to be Gaussian distributed. Convergence to a Gaussian is generally fast as $N$ increases. The Gaussian distribution is therefore commonly found in nature and it is to go-to distribution for theoreticians when they wish to describe the effect of noise on a dynamical system.

However, the Gaussian is an attractor *only if each of the constituent independent stochastic processes has a finite variance*. About a century ago mathematicians derived the attractor for when the underlying stochastic processes have an infinite variance [7–10]. The result is called a Lévy distribution or $\alpha$-stable distribution. For the characteristic function of the symmetric, zero-centered Lévy distribution, there is a concise expression:

$$\tilde{p}_\alpha(k) = \exp\left[-\sigma^\alpha |k|^\alpha\right], \tag{2}$$

where $0 < \alpha < 2$. Here $\sigma$ is a scale parameter and $\alpha$ is the so-called stability index. The scale parameter, $\sigma$, is also the amplitude of the noise term that we scaled away in Eq. (1). The characteristic function is similar to a Fourier transform $[\tilde{p}_\alpha(k) \equiv \int_{-\infty}^{\infty} p_\alpha(z) \exp[ikz]\, dz$, where $p_\alpha(z)$ is the original $\alpha$-stable distribution]. Central in this article is a Langevin equation in which the "kick magnitudes," $\xi_\alpha$, follow a Lévy distribution. We furthermore must assume throughout that the subsequent "kicks" are independent and identically distributed, i.e., that a kicksize is not correlated to a previous one and that there is no drift in the distribution of the kicksizes [11].

From Eq. (2) it is readily inferred that for $\alpha = 2$ the Gaussian is reobtained. In that case $\sigma\sqrt{2}$ is the standard deviation of the Gaussian. The case of $\alpha = 1$ leads to the well-known

 

Cauchy distribution, i.e., $p_1(z) = \sigma/(\pi(\sigma^2 + z^2))$. It can furthermore be derived from Eq. (2) that the asymptotic behavior of $p_\alpha(z)$ follows a power law:

$$p_\alpha(z) \sim \frac{\sigma^\alpha \sin(\pi\alpha/2)\Gamma(\alpha+1)}{\pi} \frac{1}{|z|^{\alpha+1}} \text{ as} |z| \to \infty, \quad (3)$$

where $\Gamma(.)$ denotes the gamma function. The power-law tail implies a slower convergence to zero as compared to the exponential tail of the Gaussian. The power-law tail is ultimately what leads to the outliers and to the divergent variance.

In Appendix A it is shown how Eq. (3) is derived. The scale parameter for $\xi_\alpha(t)$ [cf. Eq. (1)] depends on the $\Delta t$ of the discretization. The details of this dependence are also explained in Appendix A.

Over the past few decades it has become ever more clear that Lévy distributions are more than just a mathematical construct. In 1963 Mandelbrot found that the day-to-day changes of the prices of cotton stocks followed a Lévy distribution with $\alpha = 1.7$ [12,13]. In 1993 Peng *et al.* noticed that time intervals between subsequent heartbeats are also Lévy distributed [14]. Lévy distributions have been identified in solar physics [15], in climate data [16], plasma turbulence [17], etc. Very recently simulations and theoretical analysis showed that a tracer particle in a solution with active microscopic swimmers exhibits displacements with a power-law tail [18]. The common denominator for systems that exhibit Lévy distributions appears to be the *nonequilibrium* nature of these systems. Noise with a fat, power-law tail and the corresponding "extreme events" appear to be inherent to systems that convert, transport, and/or dissipate energy.

In this article we consider a noise-subjected particle in a parabolic potential (cf. Fig. 1). This setup can be taken as a model for processes where a constant driving force or a constant flux leads to a throughput, but where the system is such that fluctuations occur. A good example is a resistor through which a constant current $I$ is maintained. But due to random motion of charge carriers, the voltage across the resistor will fluctuate around $IR$, where $R$ is the resistance of the resistor [19].

For a system with a steady-state throughput, we can think of the steady state as representing a minimum of a continuous potential $U(x)$. The Taylor series around such a minimum at $x = x_*$ is $U(x) \approx U(x_*) + \frac{1}{2}U''(x_*)(x - x_*)^2 + \dots$. After setting $U(x_*) = 0$, we have a quadratic lowest-order term. For small perturbations, the cubic and higher-order terms will generally be negligible. In short, near the steady state almost any system will be driven back to the steady state by a linear restoring force.

Consider first the case where the particle in Fig. 1(a) is subjected to Gaussian distributed noise. Suppose that subsequent kicks make the particle "climb" to a height $V(x_0)$. The most probable trajectory from $x_0$ back to the vicinity of $x = 0$ is a trajectory where all the subsequent kicks have zero magnitude. This is because it is at $\xi = 0$ that the distribution has its maximum. Microscopic reversibility next implies that the most probable trajectory to "climb" to $x_0$ is the reverse of this deterministic downslide. Such an ascent would involve a "Brownian conspiracy," i.e., a number of subsequent "kicks" that are all in the same direction and of an appropriately increasing strength. Figure 1(b) shows the position as a function of time for the particle following Eq. (1) with $V(x) = x^2/40$ and time steps of $\Delta t = 1$. For the zero-average Gaussian noise we took $\sigma = 1$ (i.e., a standard deviation of $\sqrt{2}$). Four thousand time steps were simulated.

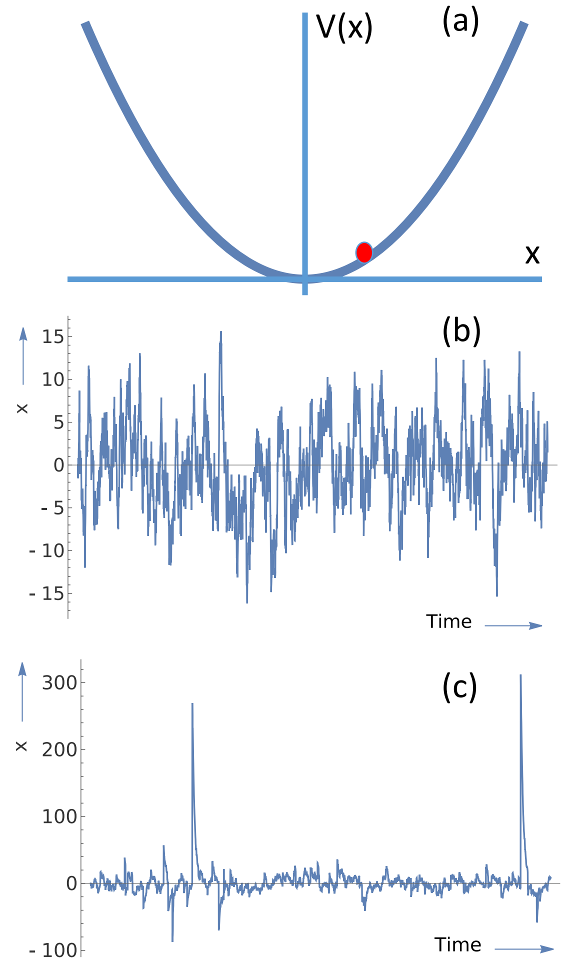


FIG. 1. (a) A noise-subjected particle in a parabolic potential $V(x) \propto x^2$. Equation (1) describes the dynamics of such a particle. (b) The positions as a function of time for when the particle is subjected to Gaussian noise, i.e., $\alpha = 2$. (c) The positions as a function of time for when the particle is subjected to Lévy noise with $\alpha = 1.5$. Further details are given in the text.

When, however, the particle is subjected to Lévy noise, the situation is very different. Microscopic reversibility no longer applies. The most likely way to downslide is still the deterministic trajectory. But the most likely way to ascend from the vicinity of $x = 0$ to $x_0$ is now one kick from the fat tail [20]. Figure 1(c) shows how this "shooting up and sliding down" scenario is followed: The large peaks represent extreme events from the tail of the distribution and involve just one time step. For each large fluctuation the subsequent relaxation back to the bottom of the parabola is much slower and involves multiple time steps. To generate Fig. 1(c) we again took $V(x) = x^2/40$ and time steps of $\Delta t = 1$. For the noise term, $\alpha = 1.5$ is the value of the stability index and $\sigma = 1$ is the value for the scale parameter. Again, 4000 time steps were simulated.

This "shooting up and sliding down" can be used to detect a deviation from time-reversal symmetry. Consider a sequence of time steps as in Figs. 1(b) and 1(c). We take the step from $j$ to $j+1$ to be a "climbing step" if $|x_{j+1}| > |x_j|$. Let $N_{\text{tot}}$ be the total number of steps in the sequence and let $N_f$ be the number of climbing steps in the sequence when the sequence is read in the forward direction. In that case the number of climbing steps in the sequence read backward is $N_b = N_{\text{tot}} - N_f$. This means that $N_b$ is also the number of descending steps if the sequence is read in the forward direction. As a measure of the time-reversal asymmetry we next adopt:

$$r = \frac{N_b - N_f}{N_f + N_b}. \tag{4}$$

The quantity $r$ is the quotient of a difference and a sum. As such, Eq. (4) has a structure that is similar to that of expressions used in optics for polarization ratio and emission anisotropy [21]. Because we are dealing with a stochastic process, we expect $r$ in our case to differ from zero even in case of microscopic reversibility [cf. Fig. 1(b)]. For $N$ tosses with a fair coin, the number of heads has an expectation value of $\frac{1}{2}N$ and a standard deviation of $\frac{1}{2}\sqrt{N}$. From this we infer that, for the case of time-reversal symmetry, the value of $r$ comes with a coefficient of variation (the ratio of standard deviation and average) of $1/\sqrt{N_{\text{tot}}}$. Only if $r$ comes out significantly larger than $1/\sqrt{N_{\text{tot}}}$ can we conclude that time-reversal symmetry is violated. The supplemental material contains two Mathematica programs to generate graphs like Figs. 1(b) and 1(c) [22]. For each run the value of $r$ is given at the end of the program. The reader can readily verify that the criterion $|r| > 1/\sqrt{N_{\text{tot}}}$ discriminates very efficiently between Gaussian and Lévy noise.

If we can decisively conclude that the noise is Lévy, then we have also ascertained that the system is nonequilibrium. Standard equilibrium features like microscopic reversibility [20] and a Boltzmann distribution [23,24] no longer apply in that case. Nonequilibrium furthermore means that the system is not isolated and is facilitating an energy transfer. If we do find the noise to be Lévy, then we also wish to be able to establish the value of $\alpha$. Below we elaborate and establish relations between $\alpha$, $r$, and the length of the time step. We will illustrate on a real-time, solar-output signal how the parameter $r$ can be used to readily determine the stability index $\alpha$ of the underlying Lévy noise.

## II. NUMERICS AND SCALING ISSUES

For $\alpha = 2$, numerical simulation of Eq. (1) is straightforward. After discretization, subsequent iterates are obtained through the application of

$$x_{i+1} = \Delta x_i + x_i, \quad \text{where} \quad \Delta x_i = \left[F(x_i) + \frac{\theta_{2,i}}{\sqrt{\Delta t}}\right]\Delta t. \tag{5}$$

Here $F(x) = -dV(x)/dx$ and $\theta_{2,i}$ is the $i$th random number drawn from a Gaussian distribution with a zero average and a scale parameter of $\sigma = 1$. Essentially, Eq. (5) represents a Euler scheme where the value of the force $F(x_i)$ is made to apply to the entire segment from $x_i$ to $x_{i+1}$. Equation (5) could become inaccurate if there is an appreciable curvature of $V(x)$ between $x_i$ and $x_{i+1}$. For the case of Gaussian noise, this problem can be overcome by taking $\Delta t$ sufficiently small. The exponential tail of the Gaussian distribution practically guarantees that there are no outliers and that $\Delta x_i$ can be kept small by choosing $\Delta t$ correspondingly small.

However, no such guarantee exists if $\alpha \neq 2$. Figure 1(c) shows several large peaks that are due to the extreme events that are characteristic of Lévy noise. These Lévy jumps obviously involve significant curvature of $V(x)$ in the course of one time step. Assume, for instance, that $x_i < 0$ and that the particle is near the bottom of the parabola where it spends most of its time. If the particle then next does a large jump to the right, i.e., $\xi_\alpha(t_i)\Delta t > 0$, then the Euler scheme would have the force due to the potential unrealistically pushing in the same direction as the kick for the entire duration of the jump.

One may be tempted to think that the problem can be overcome by taking a smaller value of $\Delta t$, but a small derivation shows that this is not the case. We first realize that $\xi_\alpha(t_i)\Delta t = \theta_{\alpha,i}\Delta t^{1/\alpha}$, where $\theta_{\alpha,i}$ is a random number drawn from a zero-centered, symmetric Lévy distribution with stability index $\alpha$ and scale parameter $\sigma = 1$. A large kick $\kappa_\alpha(t_i) = \theta_{\alpha,i}\Delta t^{1/\alpha}$ can be made smaller by a factor $\lambda$ ($\lambda > 1$) and possibly allow for Euler's linear-segment approach by taking a new $\Delta t$: $\Delta t' = \lambda^{-\alpha}\Delta t$. In the first paragraph of Appendix A it is shown how the scaling of the kicksize (which ensues from the scaling of the time interval) affects the probability distribution for the kicksizes. With the formula that is derived there, it is seen that for the tail of the distribution, where Eq. (3) applies, we have $p(\kappa_\alpha) \propto (\Delta t)p(\theta_\alpha)$. So taking smaller time steps following $\Delta t \to \lambda^{-\alpha}\Delta t$, we have for the probability density for a large kick of size $\kappa_\alpha^0$ in the tail of the distribution $p(\kappa_\alpha^0) \to \lambda^{-\alpha}p(\kappa_\alpha^0)$. If one simulates Eq. (1) over a time interval of length $T$ with a time step that is smaller by a factor $\lambda^{-\alpha}$, it implies that the number of time steps is increased by a factor $\lambda^\alpha$. So over the entire simulation, the expected number of kicks with a size between $\kappa_\alpha^0$ and $\kappa_\alpha^0 + \Delta\kappa_\alpha$ remains the same and appears independent of the length of the time step. From Eq. (3), we infer that for the probability of a kick above a certain magnitude $\xi_0$ in the positive tail, we have:

$$P_\alpha(\xi > \xi_0) \propto \xi_0^{-\alpha}. \tag{6}$$

Suppose that the original simulation with $\Delta t$ led to $n$ kicks above a size $\xi_0$. It is readily derived that the new simulation with time steps of $\Delta t'$ and a factor $\lambda^\alpha$ more time steps will on average have the same number $n$ of kicks that are larger than $\lambda\xi_0$. Ultimately, it is because of the tail's scaling property, i.e., $P_\alpha(\xi > \mu\xi_0) = \mu^{-\alpha}P_\alpha(\xi > \xi_0)$, that the problem cannot be overcome by picking the right $\Delta t$ for a discretization. All in all, for $\alpha \neq 2$ Euler's procedure is deficient.

For the parabolic potential of Fig. 1(a), there is a straightforward solution to the "large kick problem." We scale such that $V(x) = \frac{1}{2}x^2$ and come to $\dot{x} = -x + \xi_\alpha(t)$. If we let the kick at $t = t_i$ have a value $\xi_\alpha(t_i) = K$, then we can take the curvature of the potential into account by simply taking the solution of $\dot{x} = -x + K$ as describing what occurs between $x(t_i) = x_i$ and $x(t_{i+1}) = x_{i+1}$. We then find

$$x_{i+1} = (x_i - K)e^{-\Delta t} + K. \tag{7}$$

It is readily verified that for sufficiently small $\Delta t$ and $K$, the above equation reduces to the Eulerian $\Delta x_i = x_{i+1} - x_i \approx$

$(-x_i + K)\Delta t$. Figures 1(b) and 1(c) were obtained using Eq. (7) at every time step.

When numerically simulating any dynamical system, it is important that the time step $\Delta t$ is chosen to be smaller than any characteristic timescale of the system. For the Lévy-noise-driven particle in a parabolic potential, we have before any scaling operation:

$$\dot{y} = -Ay + \sigma \xi_\alpha(t), \tag{8}$$

where $A > 0$ and $\sigma$ is the amplitude of the noise. Without the noise term, Eq. (8) would describe a simple exponential relaxation with a relaxation time $t_{\mathrm{rel}} = 1/A$. The noise term, $\xi_\alpha(t)$, does not feature a characteristic timescale; it is self-similar and has the same structure on all scales. The discretization of Eq. (8) thus looks as follows: $\Delta y_i = -A\, \Delta t\, y_i + \sigma\, \theta_{\alpha,i}\, \Delta t^{1/\alpha}$. Suppose we had $A\, \Delta t \approx 1$ in the latter equation. This would lead to $\Delta y_i \approx -y_i$, even in case of $\theta_{\alpha,i}$ not yielding an outlier. If in that case a Lévy kick were to bring the particle to a large $y$, then the downslide would *not* take multiple steps. Instead, the return to the bottom of the potential would generally require just one step. Taking a dimensionless time, i.e., $\Delta\tau = A\, \Delta t$, and taking $y = (\sigma/A^{1/\alpha})x$, we come to a completely dedimensionalized equation: $\Delta x_i = -x_i\, \Delta\tau + \theta_{\alpha,i}\, \Delta\tau^{1/\alpha}$. Of course, $\Delta\tau \ll 1$ is required for realistic simulation.

Finally, it is worth noting that for $\Delta t \to \infty$, Eq. (7) yields $x_{i+1} = K$. This means that the location $x_{i+1}$ is completely independent of the location $x_i$ at the previous time step. The ensuing symmetry would lead to $r \to 0$ for $\Delta t \to \infty$.

## III. THEORY FOR THE TIME-REVERSAL ASYMMETRY PARAMETER *r*

### A. The fractional Fokker-Planck equation

In the previous sections we analyzed an ordinary differential equation with a stochastic input. However, it is possible to formulate an equivalent partial differential equation for how the probability distribution, $P(x,t)$, evolves in time. For the case of Gaussian noise, it is well known how a Langevin Equation can be turned into a Fokker-Planck Equation [25]. That traditional Fokker-Planck Equation has a first derivative with respect to the position $x$ to describe drift terms and a second derivative with respect to $x$ that describes the diffusion. For the case of Lévy noise, a noninteger value of the stability index $\alpha$ leads to a so-called fractional Fokker-Planck equation, i.e., a Fokker-Planck equation with, instead of a second derivative, a noninteger derivative. The fractional Fokker-Planck equation corresponding to Eq. (8) is [26]

$$\frac{\partial P(x,t)}{\partial t} = A \frac{\partial [xP(x,t)]}{\partial x} + \sigma^\alpha \frac{\partial^\alpha P(x,t)}{\partial |x|^\alpha}. \tag{9}$$

After setting the left-hand side equal to zero, a stationary solution can be obtained. Fractional derivatives become multiplicative factors in Fourier space, i.e., $\frac{\partial^\alpha}{\partial|x|^\alpha} f(x) = -\int_{-\infty}^{\infty} \frac{dk}{2\pi} e^{ikx} |k|^\alpha \tilde{f}(k)$, where $\tilde{f}(k)$ is the Fourier transform of $f(x)$. The factor $x$ in the numerator of the first term on the right-hand side of Eq. (9) leads to the factor $\frac{\partial}{\partial k}$ in Fourier space. So at steady state we have the following equation in

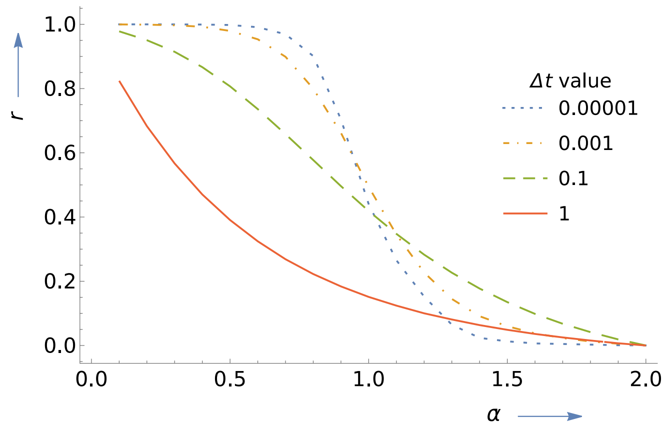


FIG. 2. (a) The time-reversal asymmetry parameter, $r$ [cf. Eq. (4)], versus the stability index, $\alpha$, that characterizes the noise. The curves result from stochastic simulations of $\dot{x} = -x + \xi_\alpha(t)$ through the ensuing Eq. (7). Curves are drawn for different values of the time interval $\Delta t$. Values of $\alpha$ were taken in increments of 0.1 and each point is the result of a simulation with $N_{\mathrm{tot}} = 10^7$ time steps [cf. Eq. (4)].

Fourier space:

$$-Ak\frac{d\tilde{P}_{\mathrm{st}}(k)}{dk} - \sigma^\alpha |k|^\alpha \tilde{P}_{\mathrm{st}}(k) = 0. \tag{10}$$

This equation is readily solved:

$$\tilde{P}_{\mathrm{st}}(k) = \exp\left[-\frac{\sigma^\alpha |k|^\alpha}{A\alpha}\right]. \tag{11}$$

We see that for $\alpha \neq 2$ the probability density function for the position in the parabola is not the Boltzmann distribution that would ensue at equilibrium. Instead it is again an $\alpha$-stable distribution. The stability index $\alpha$ is the same as it is for the distribution of the kicks, but the scale parameter has changed: from $\sigma$ to $\sigma' = \sigma/(A\alpha)^{1/\alpha}$. For a fully scaled system, i.e., $A = 1$ and $\sigma = 1$, we have

$$\tilde{p}(k) = \exp[-|k|^\alpha] \tag{12}$$

for the kicksize distribution and

$$\tilde{P}_{\mathrm{st}}(k) = \exp[-|k|^\alpha/\alpha] \tag{13}$$

for the position distribution. Relating the latter equation to Eq. (2), we see that $\tilde{P}_{\mathrm{st}}(k)$ comes with a scale parameter $\sigma' = (1/\alpha)^{1/\alpha}$.

It is important to be aware that the distributions (12) and (13) will only emerge from a simulation with an infinitesimally small time interval, i.e., $\Delta t \to 0$. As was noted already at the end of last section, the other limit, i.e., $\Delta t \to \infty$, leads to the position distribution being identical to the kick distribution and thus $\tilde{P}_{\mathrm{st}}(k) = \tilde{p}(k)$ for all values of $\alpha$.

The $\alpha$ in the denominator of the exponent of Eq. (13) translates into the kicksize distribution, $p(\xi)$, and the position distribution, $P_{\mathrm{st}}(x)$, differing solely by a scaling factor $\sigma'$ (see Appendix A), i.e.,

$$P_{\mathrm{st}}(x) = \frac{1}{\sigma'} p\left(\frac{x}{\sigma'}\right). \tag{14}$$

Figure 2 shows how the time-reversal asymmetry parameter, $r$, depends on the stability index, $\alpha$. The curves are derived from stochastic simulations [cf. Eq. (7)] of a scaled ($A = 1$ and $\sigma = 1$) Langevin equation. It is obvious that reality bears out what was explained in the last section: for higher values of $\Delta t$, the curves move toward $r = 0$. It is furthermore observed that the $r$-vs.-$\alpha$ curves are sigmoids where $r$ goes from an $r = 1$-plateau to an $r = 0$-plateau as $\alpha$ increases. The inflection points appear close to $\alpha = 1$. For $\Delta t \to 0$ the sigmoid converges to a step function.

### B. The $\alpha = 2$ case

For $\alpha = 2$, the statistics are not "polluted" by Lévy jumps. We take $\Delta t$ to be sufficiently small for the Euler scheme approximation to Eq. (1) to apply. The piecewise-linear solution that the Euler scheme gives will be more accurate as $\Delta t$ is taken smaller. For the increments we have

$$\Delta x_i = -x_i \Delta t + \theta_{\alpha=2,i}\sqrt{\Delta t}, \tag{15}$$

where $\theta_{\alpha=2,i}$ is the $i$th random number drawn from a distribution with $\sigma = 1$. From Eq. (15) it is obvious that, for one particular time step, the deterministic part of the motion becomes negligible if $\Delta t \to 0$. In that case $(\Delta x)^2$ and $\Delta t$ are of the same order, i.e., $(\Delta x)^2 \sim \Delta t$. We take two nearby points, $x$ and $x + \Delta x$, where $x > 0$ and $\Delta x > 0$. We next focus on the particles that move between these points in *exactly* $\Delta t$. If microscopic reversibility applies, then the traffic in both directions should be equal. From Eq. (15) we find that in order to move from $x$ to $x + \Delta x$ in time $\Delta t$, a kick $\theta_{\alpha=2,i} = x\sqrt{\Delta t} + \Delta x/\sqrt{\Delta t}$ is required. In order to move from $x + \Delta x$ to $x$ in $\Delta t$, we need $\theta_{\alpha=2,i} = (x + \Delta x)\sqrt{\Delta t} - \Delta x/\sqrt{\Delta t}$. Taking into account the different probability densities, $P_{\rm st}$, at $x$ and $x + \Delta x$, we find for the difference, $\hat{r}$, between descending and ascending traffic:

$$\begin{aligned}\hat{r} &= P_{\rm st}(x + \Delta x)p[(x + \Delta x)\sqrt{\Delta t} - \Delta x/\sqrt{\Delta t}] \\ &\quad - P_{\rm st}(x)p(x\sqrt{\Delta t} + \Delta x/\sqrt{\Delta t}).\end{aligned} \tag{16}$$

Note that $\hat{r}$ is different from $r$ [cf. Eq. (4)] in that it is local and has a dimension of square density. Next substituting $P_{\rm st}(x) = 1/\sqrt{2\pi}\exp[-x^2/2]$ and $p(x) = 1/(2\sqrt{\pi})\exp[-x^2/4]$ for the position distribution and the kicksize distribution, respectively, we infer after some algebra:

$$\begin{aligned}\hat{r} &\propto \exp\left[-\frac{1}{2}x^2 - \frac{1}{4}\frac{(\Delta x)^2}{\Delta t} - \frac{1}{2}x(\Delta x) - \frac{1}{4}x^2(\Delta t)\right] \\ &\quad \times \left\{\exp\left[-\frac{1}{4}(\Delta x)(\Delta t)(2x + \Delta x)\right] - 1\right\}.\end{aligned} \tag{17}$$

For $(\Delta x)^2 \sim \Delta t$, only the first two terms in the exponent in the prefactor are finite. The second exponential term, the one in the round brackets, has terms in the exponent that can all be made arbitrarily small by picking $\Delta x$ and $\Delta t$ sufficiently small. We thus find that $\hat{r}$ approaches zero as $\Delta t \to 0$ and $\Delta x \to 0$. Every trajectory between any two points $(t_1, x_1)$ and $(t_2, x_2)$ can be constructed from small linear steps that each have $\hat{r} \to 0$. It can be concluded that microscopic reversibility applies for Gaussian noise. We thus also have $r = 0$ [cf. Eq. (4)] for $\alpha = 2$.

### C. Lévy flights

In case of a Lévy flight, the particle "shoots up" from a basin of attraction near $x = 0$, and subsequently "slides down" [20]. These "flights" occur for $0 < \alpha < 2$, they break microscopic reversibility, and they lead to $r > 0$.

Consider the following one-dimensional (1D) situation. Particles are moving from a reservoir A to a reservoir B at a speed that is 10 times as large as the speed with which they are moving from B to A. The number of particles in the reservoirs A and B stays constant. The latter fact implies for the fluxes: $J_{A\to B} = J_{B\to A}$. The identical fluxes and tenfold different speeds can only be achieved if, at any time, the number of particles that is moving along in the $B \to A$ direction is 10 times the number of particles moving in the $A \to B$ direction.

So with a stationary Lévy distribution in the parabolic potential, there are, at any time, more descending steps taking place than climbing steps.

### D. The case of $\alpha \neq 2$

Let $P_{\rm climb}(x)$ be the probability that, for a particle at position $x$, the next step brings the particle to a higher position in the parabola. For the fraction of steps that are climbing steps, $\varphi_{\rm climb}$, we then have

$$\varphi_{\rm climb} = \int_{-\infty}^{\infty} P_{\rm climb}(x)P_{\rm st}(x)\,dx, \tag{18}$$

where $P_{\rm st}(x)$ is the stationary probability-density distribution for which $\tilde{P}_{\rm st}(k)$, cf. Eq. (11), is the generating function. The parameter $r$ is related to $\varphi_{\rm climb}$ through

$$r = 1 - 2\varphi_{\rm climb}. \tag{19}$$

The argument presented in the previous paragraph makes clear that, for $0 < \alpha < 2$, we should have $0 < \varphi_{\rm climb} < 1/2$ and, consequently, $0 < r < 1$.

For positive $x_i$, the probability $P_{\rm climb}(x_i)$ can be split out as follows: $P_{\rm climb}(x_i) = P(x_{i+1} > x_i) + P(x_{i+1} < -x_i)$. With Eq. (7) this means that the kicksize, $K$, has to follow either $K > x_i$, or $K < -sx_i$, where

$$s = \frac{e^{\Delta t} + 1}{e^{\Delta t} - 1}. \tag{20}$$

Generalizing to any real $x$, it is thus found that

$$\varphi_{\rm climb} = \int_{-\infty}^{\infty}\left[\int_{-\infty}^{-sx} p(\xi)\,d\xi + \int_{x}^{\infty} p(\xi)\,d\xi\right]P_{\rm st}(x)\,dx. \tag{21}$$

The inner integrals can be replaced by their respective cumulative distribution functions (which are available in Mathematica). The symmetry in $x$, furthermore, allows us to integrate over half the domain and double the result:

$$\varphi_{\rm climb} = 2\int_{0}^{\infty} [{\rm cdf}(sx) + {\rm cdf}(x)]P_{\rm st}(x)\,dx. \tag{22}$$

We affirmed the validity of our derivations by successfully replicating Fig. 2 using, instead of the Monte Carlo approach, Eqs. (19), (20), and (22) (not shown).

There are no simple and general analytic formulas to describe the curves in Fig. 2. However, there are some approximations that can help understand and intuit the curves. There appears to be a "transition" at $\alpha = 1$. This can be understood as follows. For the probability of a kick that makes the particle reach into the tail between positions at $x$ and $x + \Delta x$ we have $\Delta P \propto x^{-\alpha-1}\Delta x$. Through integration we find how far the average extreme event reaches: $\langle x\rangle \propto \int^{\infty} x\, x^{-\alpha-1}\, dx \propto x^{-\alpha+1}|^{\infty}$. This integral is infinite for $0 < \alpha < 1$ and finite for $1 < \alpha < 2$.

### E. The $\alpha = 1$ case

Only for $\alpha = 1$ are the kicksize distribution, cf. Eq. (12), and the position distribution, cf. Eq. (13), identical. For this case it is easily proven that $r = 1/2$ if $\Delta t \to 0$. Taking $f(x) = \int_{\xi=x}^{\infty} p(\xi)\, d\xi$ and next realizing that $f(0) = 1/2$ and $f(x \to \infty) = 0$, we see how the integral Eq. (21) reduces:

$$\begin{aligned} \varphi_{\text{climb}} &= 2\int_{x=0}^{\infty}\left[\int_{\xi=x}^{\infty} p(\xi)\, d\xi\right] p(x)\, dx \\ &= 2\int_{x=0}^{\infty}\left[\int_{\xi=x}^{\infty} p(\xi)\, d\xi\right]\left[-\frac{d}{dx}\int_{\xi=x}^{\infty} p(\xi)\, d\xi\right] dx \\ &= -2\int_{x=0}^{\infty} f(x) f'(x)\, dx = -f^2(x)|_{x=0}^{\infty} = \frac{1}{4}. \end{aligned} \tag{23}$$

With Eq. (19), this result leads to $r = 1/2$.

Through Eqs. (21) and (22) it is even possible to obtain an analytic result for $\varphi_{\text{climb}}^{\alpha=1}$ for a finite $\Delta t$. The Mathematica package readily gives the analytic result:

$$\varphi_{\text{climb}}^{\alpha=1} = \frac{1}{8} + \frac{\Phi\left(\frac{1}{s^2}, 2, \frac{1}{2}\right)}{4\pi^2 s} + \frac{\log(s)\coth^{-1}(s)}{\pi^2}, \tag{24}$$

where $\Phi(.,.,.)$ represents the so-called Lerch transcendent, i.e., $\Phi(z, s, \beta) = \Sigma_{n=0}^{\infty} z^n/(n+\beta)^s$. In agreement with what Fig. 2 shows, this analytic result has $r$ going down from $r = 1/2$ to $r = 0$ as $\Delta t$ gets larger.

### F. The $\alpha \to 0$ case

For $\alpha = 0$ the generating function is a constant and this implies that the probability distribution is a Dirac delta function. In the $\alpha \to 0$ limit the probability distribution looks like a sharp spike at $x = 0$ with power-law tails. From Fig. 2 it appears that the climbing fraction $\varphi_{\text{climb}}$ approaches zero in the $\alpha \to 0$ limit. Going back to Eqs. (13) and (14), we see that the $\alpha$ in the denominator of the exponent in $\tilde{P}_{\text{st}}(k)$ [cf. Eq. (13)] translates into a scaling factor $\sigma' = (1/\alpha)^{1/\alpha}$ for $P_{\text{st}}(x)$. This means that for $\alpha \to 0$, the position distribution $P_{\text{st}}(x)$ is wider than the kicksize distribution $p(\xi)$ by a very large factor. How this leads to $\varphi_{\text{climb}} \to 0$ can be understood from a Langevin perspective by realizing that after a large Lévy jump that drives the particle high up the parabola, it will, at $\Delta t \to 0$, take an infinite number of time steps to slide down again. In the context of Eqs. (21) and (22), the $\varphi_{\text{climb}} \to 0$ result can be understood after realizing that cdf$(x)$ decreases from 0.5 to 0 as $x$ increases from $x = 0$. If $P_{\text{st}}(x)$ is much wider than $p(\xi)$, then cdf$(x)$ will be effectively zero for most of the relevant domain of $P_{\text{st}}(x)$ and $\varphi_{\text{climb}} = 0$ will result.

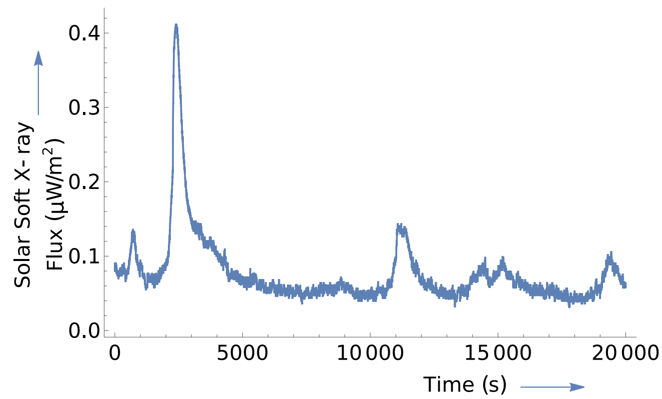


FIG. 3. An approximately 6-h record of solar x-ray fluxes sampled at 2-s intervals. Data were recorded by the Geostationary Operational Environmental Satellite series and are published online [33]. x-rays were recorded in a window between 1 and 8 Å, the "soft" regime.

## IV. PRACTICAL APPLICATIONS

Different methods are available to estimate the parameters of the $\alpha$-stable distribution that best fits a set of observed data [27,28]. The maximum likelihood method is popular and easy to understand [29]. However, it is not a realistic option for very large data sets as the matrices involved in the computation become unmanageably large. The quantile method is also relatively straightforward: It compares observed-data histograms to prior tabulations [30]. It is fast and appropriate for large data sets. In Ref. [31] a Fast Fourier Transform is used to generate a characteristic function of the observed data. Fitting parameters is next done in Fourier space where the $\alpha$-stable distributions are mathematically more easily expressed. Reference [27] compares these methods. For a very large data set there may be sufficiently many extreme events that the power-law tail [cf. Eq. (3)] can be used to estimate $\alpha$. In Ref. [32] this idea is applied to solar soft x-ray emission data (cf. Fig. 3).

We propose that establishing the value of $r$ from the observed data and next using the patterns observed in Fig. 2 to determine the value of $\alpha$ is in many cases a simple, robust, and effective method. Our method is suitable in case of a data stream as in Fig. 1(c), i.e., a data stream that exhibits large jumps. These jumps are to have power-law-distributed magnitudes and are to be followed by a slower relaxation back to the baseline. This is indicative of Lévy noise in a parabola [cf. Fig. 1(a)] being the appropriate model. As was pointed out before, with a parabolic potential the $\alpha$ that characterizes the position distribution $P_{\text{st}}(x)$ is the same as the $\alpha$ that characterizes the noise term $\xi_\alpha(t)$. In determining the value of $r$, we are taking differences between subsequent numbers in a time sequence. So in our method the order of the sampled data points is essential. The methods described in the previous paragraph also apply to the $\xi_\alpha$ of Eq. (1). To assess $\xi_\alpha$, numbers can then be taken in any order as they are presumed to be independent and identically distributed.

In Figs. 1(b) and 1(c) it is the value of $x$ that constitutes the signal that is followed over time. It should be noticed that if the value of $x^2$ is followed instead, climbing steps remain climbing steps and nonclimbing steps remain nonclimbing steps, i.e., the value of $r$ is not affected. As a matter of fact, for any odd or even $f(x)$ where $f(x)$ is increasing for $x > 0$, the same value for $r$ ensues.

With a simulation as in Fig. 1 it is unambiguous whether a step is a climbing step or not. After all, we know that $x = 0$ represents the bottom of the parabolic potential. In a real-life sequence of noisy data, however, it may be difficult to establish the precise location of the point $x_*$ where the potential has its minimum. The particle spends the vast majority of its time near the bottom of the parabola and a small variation in the estimate of the $x = x_*$ point, i.e., moving the horizontal axis in Figs. 1(b) and 1(c) a little up or down, will for many steps affect the assessment whether the step is "climbing" or not. Taking the average value of the data sequence as the $x = x_*$ point is not a solution even if the number of data points is very large. This is because the average converges slowly or not at all if data have an $\alpha$-stable distribution. An additional problem occurs when there is a tiny shift in the value of $x_*$ in the course of the data collection.

No vagueness in the estimate of $x_*$, however, occurs when working with a data stream that can be identified with values that are proportional to $z = (x - x_*)^2 + Z_0$, where $Z_0$ is a constant. In that case the lowest value of the signal in the entire sequence can be safely taken as representing the bottom of the parabola. Any increase of the signal value from one sample point to the next can then be unambiguously counted as a climbing step. Obviously this applies for any $z = f(x - x_*) + Z_0$ where $f$ is a function that monotonically increases on $(x - x_*) > 0$ and monotonically decreases on $(x - x_*) < 0$. As a first example to illustrate this, think of a room with a thermostat. If the room gets too cold, then an air conditioner is turned on. If the room gets too hot, then a heater is turned on. The power consumption, as given by the electric meter, will always be positive. As a second example, think of an airplane with mass $m$ for which gravity and the lift force are in balance when the plane flies at an altitude $h_0$ at a horizontal velocity $v_0$. There is a restoring force toward $h_0$; if the plane increases (decreases) altitude, the decreased (increased) air density will decrease (increase) the lift force. Let $\Delta v$ be the vertical velocity due to the altitude fluctuations and the restoring force. The kinetic energy of the plane relative to a point on the ground is $E_{\rm kin} = \frac{1}{2}m(v_0^2 + \Delta v^2)$ and has the form presented in the first sentence of this paragraph.

Figure 3 shows 6 hours of solar soft x-ray flux as captured by satellite. X-ray fluxes are central in the study of solar flares [34]. A record of solar soft x-ray fluxes going back many years is publicly available through the website of the National Oceanic and Atmospheric Administration. Outliers and a characteristic "shooting up and sliding down" are evident in Fig. 3. It is also clear that the sampling rate is fast compared to the rate of relaxation as the relaxation after a spike lasts a few thousand seconds. This allows for an analysis related to Fig. 2 in Sec. III.

The differential rotation of the Sun and the convective flows in the Sun's interior stretch and wrap the magnetic field lines. As the solar cycle progresses the field-line pattern gets more twisted. Solar flares occur as a result of magnetic reconnections, i.e., the field reconfiguring itself and transitioning to a lower energy structure [35,36]. The peaks in Fig. 3 can be

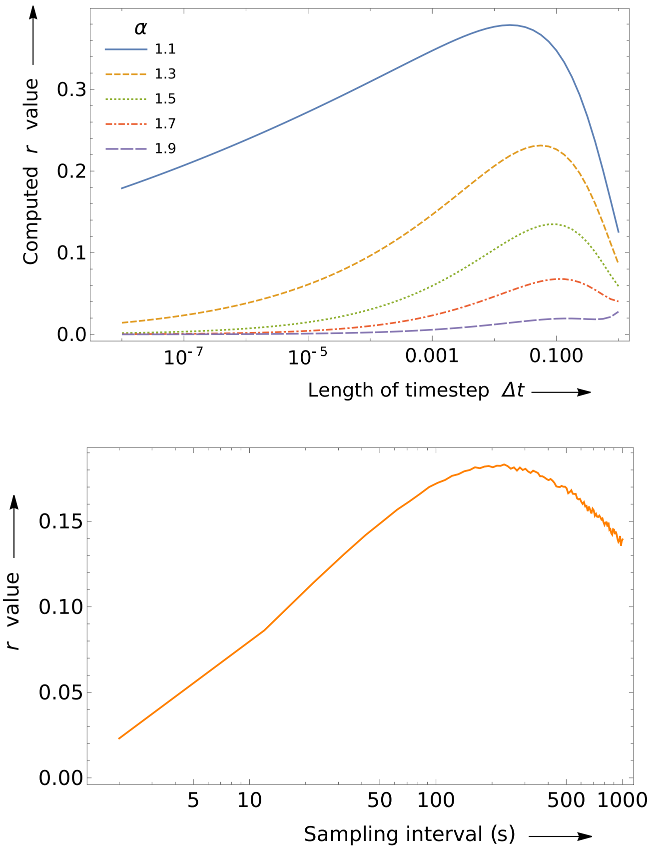


FIG. 4. The values of $r$ calculated by undersampling. The top figure (a) shows theoretical results following Eqs. (18)–(22) for different values of $\alpha$ with $1 < \alpha < 2$. The bottom figure (b) derives from solar soft x-ray data as shown in Fig. 3 and computed in intervals of 10 s.

associated with solar flares. The distributions of observable quantities that are connected to solar flares have been found to follow power laws [37].

A solar flare's x-rays are in fact bremsstrahlung and thermal radiation (at $>10^6$ K). These are emitted directly following the explosive release of the reconnection energy. As the energy disperses and dissipates there is ultimately a return to the nonequilibrium steady-state. Figure 3 shows the watts per square meter that the detector receives. It is not unreasonable to identify the jump and subsequent relaxation in Fig. 3 with a Lévy jump and a subsequent decrease of $V(x)$ in Fig. 1(a). But, as was mentioned before, the same value for $r$ is obtained for any signal that is proportional to $z$ where $z = f(x) + Z_0$ with $f'(x) > 0$ on $x > 0$ and $f'(x) < 0$ on $x < 0$. What matters is that the underlying process giving rise to the movement of $x$ is the noisy particle in the parabolic potential, i.e., Eq. (1) and Fig. 1(a).

The relaxations that are apparent in Fig. 3 indicate that Eq. (1) and Fig. 1(a) are the right model. The power laws associated with solar flare occurrence tell us that we have Lévy jumps, i.e., $\alpha < 2$.

In Fig. 2 it is apparent that for $\alpha > 1$ the value of $r$ does not change monotonically with the time step length $\Delta t$. There appears to be a peak for $\Delta t \approx 0.1$. Here we further explore this feature to establish $\alpha$ for solar soft x-ray fluxes. Figure 4(a) derives from the theoretical analysis using Eqs. (18)–(22) and shows $r$ as a function of $\Delta t$ for different values of $\alpha$. The apparent maximum can be intuited as follows. To the right of the maximum the number of time steps in a relaxation back to the baseline after a peak, i.e., the number of descending steps, decreases as $\Delta t$ is made larger. To the left time steps get smaller when moving away from the maximum. The displacement $\Delta x$ during a time step is the result of both drift and diffusion. The contributions due to drift and diffusion are

$$\Delta x_{\mathrm{drift}} \propto \Delta t \quad \text{and} \quad \Delta x_{\mathrm{diff}} \propto \Delta t^{1/\alpha}, \tag{25}$$

respectively. With $1 < \alpha < 2$ it is obvious that for an individual step the diffusive contribution takes on a greater significance if $\Delta t$ is brought closer to zero. So for $\Delta t \to 0$ diffusion overwhelms drift and the probabilities to be climbing and descending both approach $1/2$. A complete relaxation from a peak back to the baseline will contain more descending steps than climbing steps, but for decreasing $\Delta t$ that difference will be an ever smaller fraction of the total number of steps involved in the relaxation. As a consequence Eq. (4) will yield a smaller value for $r$. It should also be realized that information about steplength is erased when merely counting ascending and descending steps. When relaxing back from a peak to the baseline, the required net descent also occurs when descending and climbing steps are equal in number, but with descending steps being on average longer than climbing steps. Finally, we mention that the above Eq. (25) also explains why the method described in this section no longer applies if $\alpha < 1$.

The $\alpha$ parameter for solar soft x-ray fluxes has also been estimated through scaling properties associated with the power-law tails for $\alpha < 2$ [32]. A block of data that is twice as long will on average yield a maximum value that is a factor $2^{1/\alpha}$ larger [38]. The slope in a log-log plot of the average maximum value against the block size, next gives the value of $1/\alpha$. We took the data for the years 2011–2016. These years represent a solar maximum during which the flare activity appears fairly constant [32]. Because lengths of data blocks must be powers of two, we ended up cutting off seven months at each end. Using the method of Ref. [32] we thus reproduced the $\alpha = 1.22$ that was also in Ref. [32] for prior solar cycles.

Figure 4(b) shows results from measurements of solar soft x-rays. The figure derives again from the 2011–2016 solar maximum with seven months cut off at each end. The shape is visually congruent to shapes seen in Fig. 4(a). The location of the maximum also corresponds well—it occurs at a timescale close to a tenth of the observable relaxation time after a peak (cf. Fig. 3). An interpolation of this maximum between the curves of Fig. 4(a) leads to an estimate of $\alpha = 1.38$ for the solar soft x-ray flux. In Appendix B we present a step-by-step algorithm to extract the value of $\alpha$ from a stream of sampled data. Our $\alpha = 1.38$ appeared very robust; the same value was found when shorter slices of data (single years or months) were taken. Other methods appeared less robust in their $\alpha$-estimate when subsets of the entire record were taken (data not shown).

Applying the quantile method [39] to the 2011–2016 solar maximum with seven months cut off at each end, it is found that $\alpha = 1.26$. Quantile-method-estimates for shorter slices of the data appear quite variable. This is likely a reflection of fact that the quantile method estimates more than just the $\alpha$; the scale parameter, baseline level, and skew of the distribution are also involved and these may drift over time.

Both our $r$ value method and the power-law-tail method of Ref. [32] are aimed at the value of the stability index $\alpha$. Nevertheless, a drift in the scale parameter $\sigma$ affects the ultimate estimate for $\alpha$. For the power-law-tail method it is obvious from Eq. (3) that a change of $\sigma$ during the data stream will "contaminate" the estimate for $\alpha$. For our $r$ value method the parameter $A$ that characterizes the parabolic potential [cf. Eq. (8)] is ultimately incorportated in the scale parameter for $P_{\mathrm{st}}(x)$ (see Sec. III). But $A$ also gives the relaxation time $t_{\mathrm{rel}} = 1/A$. A drift in the relaxation time will shift the maximum in Fig. 4(b) to the left or right and can thus affect the estimate for $\alpha$.

Finally, it is interesting to note that the power-law-tail method of Ref. [32] derives its estimate from the numerical values of the outlier data. The vast majority of the data is effectively not utilized. The order in which the numbers occur is also not used. Our $r$ method exploits the entire data sequence, but discards exact numerical values and focusses on just the sign of the difference between two subsequent data points.

## V. RESULTS AND DISCUSSION

It has long been understood that microscopic reversibility does not apply for a system that is out of equilibrium. Violation of microscopic reversibility means that forward- and backward time are distinguishable. Different approaches have been tried to understand, detect, and quantify the "Arrow of Time." Very recently a method involving the Fluctuation Theorem was presented [40]. Much work on nonequilibrium and irreversibility has focused on entropy. For two probability distributions $p(x)$ and $q(x)$, the Kullback-Leibler divergence (KLD), or relative entropy, is expressed as $D[p(x)||q(x)] = \int dx\, p(x) \ln(p(x)/q(x))$. Because the KLD is always positive and vanishes if $p(x) = q(x)$ for all $x$, it can be intuited as a "distance" between the two probability distributions [41,42]. For our noisy particle in a parabolic potential, it can be used to put a scalar value on the difference between the Boltzmann distribution at equilibrium (i.e., $\alpha = 2$ and $r = 0$) and the Lévy distribution [cf. Eq. (13)] at nonequilibrium (i.e., $0 < \alpha < 2$ and $0 < r < 1$). In this way the KLD is like the $r$ and a more explicit connection could possibly be derived. In this context it also needs to be pointed out that the nonequilibrium for $0 < \alpha < 2$ involves continuous input of energy and production of entropy.

In this paper we took a basic and generic system: a noisy, overdamped particle in a parabolic potential. The nonequilibrium feature consisted in the particle being subjected to Lévy noise instead of Gaussian noise. With the parameter $r$ [cf. Eq. (4)] we developed a way to quantitatively assess the deviation from time-reversal symmetry. The stability index $\alpha$ characterizes the Lévy noise. For $\alpha = 2$ the noise is Gaussian. In that case we have time-reversal symmetry and $r = 0$. Figure 2 shows how $r$ goes to one as we break time-reversal symmetry and go from $\alpha = 2$ to $\alpha = 0$. The figure also shows how the value of $r$ depends on the choice of the time interval $\Delta t$ for the simulation.

It is remarkable and useful that the value of $r$ stays the same when the time signal that is being followed is not the $y$ in Eq. (8), but an odd or even function $f(y)$ where $f'(y) > 0$ for $y > 0$. The value of $r$ readily leads to the stability index $\alpha$ that characterizes the underlying Lévy noise term $\xi_\alpha(t)$ [cf. Eq. (8)]. A good estimate for $\alpha$ is essential in identifying the physics taking place at the source of a signal. The method that we developed in Sec. IV of this article yields a reliable estimate of $\alpha$ from a real-life time series. Our method could more generally be helpful in the analysis of nonequilibrium systems, not just in astrophysics, but also in geology, physiology, climate science, economics, etc.

## ACKNOWLEDGMENTS

We are grateful to Ł. Kuśmierz for useful comments on earlier versions of the manuscript.

## APPENDIX A: SCALING ISSUES WITH THE α-STABLE DISTRIBUTION

When a stochastic variable $\zeta$ is multiplied with a factor $\lambda$ ($\lambda > 1$), the distribution for $\zeta' = \lambda\zeta$ is wider and has a scale factor (or standard deviation) that is $\lambda$ times larger. How the probability distributions $p(\zeta)$ and $p'(\zeta')$ are related is easily derived from $p'(\zeta')\,d\zeta' = p(\zeta)\,d\zeta$. We find $p'(\zeta') = (1/\lambda)\,p(\zeta'/\lambda)$. This result makes sense after the realization that the horizontal stretching by a factor $\lambda$ (the dividing by $\lambda$ in the argument) must be accompanied by a vertical compression (the $1/\lambda$ prefactor) to maintain normalization.

For $k \to 0$ the characteristic function $\tilde{p}_\alpha(k) = \exp[-\sigma^\alpha |k|^\alpha]$ [cf. Eq. (2)] can be approximated by:

$$\tilde{p}_\alpha(k) \approx 1 - \sigma^\alpha |k|^\alpha. \tag{A1}$$

The probability distribution $p_\alpha(z)$ is related to the characteristic function $\tilde{p}_\alpha(k)$ through $p_\alpha(z) = \frac{1}{2\pi}\int_{-\infty}^{\infty} \tilde{p}_\alpha(k) \exp[-ikz]\,dk$. For $k \to 0$ the product $kz$ in the exponent will only differ significantly from zero if $z \to \infty$. It is therefore that the $k \to 0$ limit corresponds to the $z \to \infty$ limit. The second term in Eq. (A1) readily leads to the power-law Eq. (3).

Consider an overdamped free particle. When subject to Lévy noise, the particle's motion is described by $\dot{x} = \sigma\xi_\alpha(t)$. The Lévy noise term, $\xi_\alpha(t)$, has structure on all scales. Because of this, the discrete time steps $\Delta t$ that are necessary for a simulation include a scale factor for $\xi_\alpha(t)$ that depends on $\Delta t$. We have $\xi_\alpha(t_i)\,\Delta t = \theta_{\alpha,i}(\Delta t)^{1/\alpha}$, i.e., $\xi_\alpha(t_i) = \theta_{\alpha,i}(\Delta t)^{(1-\alpha)/\alpha}$. Here $\theta_{\alpha,i}$ denotes the $i$th random number drawn from a zero-centered, symmetric Lévy distribution with stability index $\alpha$ and unity scale parameter. It is obvious from here that the amplitude $(\Delta t)^{1/\alpha}$ is like the scale factor $\lambda$ in the first paragraph of this Appendix.

For an $\alpha$-stable distribution with a unity scale factor we have for large $|\theta|$:

$$p_\alpha(\theta) \sim \frac{\sin\left(\frac{\pi\alpha}{2}\right)\alpha\Gamma(\alpha)}{\pi} \frac{1}{|\theta|^{\alpha+1}} \quad \text{as} |\theta| \to \infty. \tag{A2}$$

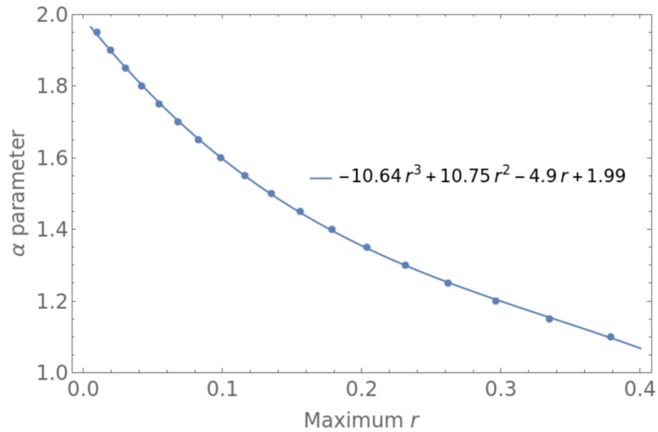


FIG. 5. The value of $r$ exhibits a maximum on variation of $\Delta t$ (or, equivalently, the sampling rate). The exact value of $r$ at the maximum depends on the stability index $\alpha$ [cf. Fig. 4(a)]. The above curve leads from the observed $r$-maximum to a corresponding estimate for $\alpha$ for $1.1 \lesssim \alpha \lesssim 1.95$. The points were obtained through Eq. (22). The curve is a cubic-polynomial fit to these points.

In a simulation with a time step $\Delta t$, we have $\kappa_\alpha(t_i) = \xi_\alpha(t_i)\Delta t = \theta_{\alpha,i}(\Delta t)^{1/\alpha}$ for the random kicks. Realizing that $\Delta t^{1/\alpha}$ is the scale factor that connects $\kappa_\alpha(t_i)$ and $\theta_{\alpha,i}$, and next applying the result that was derived in the first paragraph of this Appendix, we infer for the asymptotic behavior of the distribution $p_\alpha(\kappa)$:

$$p_\alpha(\kappa) \sim \frac{\Delta t\,\sin\left(\frac{\pi\alpha}{2}\right)\alpha\Gamma(\alpha)}{\pi} \frac{1}{|\kappa|^{\alpha+1}} \quad \text{as} |\kappa| \to \infty. \tag{A3}$$

This implies that the term $\sigma^\alpha$ in Eq. (3) can be identified with $\Delta t$. For the scale factor $\sigma$ we thus have $\sigma = (\Delta t)^{1/\alpha}$.

## APPENDIX B: ALGORITHM TO EXTRACT α FROM A STREAM OF SAMPLED DATA

As discussed in Sec. IV, the value of $r$ is enhanced for sampling rates just above the characteristic scale of a system. For series that encompass this range, an estimate for $\alpha$ can be obtained by comparison with theoretical values computed via Eq. (22), which are unique for $1.1 \lesssim \alpha \lesssim 1.9$ (cf. Fig. 4). Numerically calculated maximum-$r$ values are shown in Fig. 5, along with a polynomial fit. For a series $X$ with a zero value corresponding to the position at the bottom of the parabolic potential, the estimation is done as follows:

(i) Create a set of undersampled series $X_n$'s by taking every $n$th value for $n = 1, 2, 3, \ldots$.

(ii) For each $X_n$, calculate $r_n$ according to Eq. (4), i.e.,

(a) Take the absolute value of each element.

(b) For each element, subtract the subsequent element.

(c) For the ensuing differences, subtract the number of negative values from the number of positive values.

(d) Divide by the length of $X_n$ minus 1.

(iii) Find the maximum $r_n$, which should correspond to a peak in the trend of the ordered $r_n$ values (as in Fig. 4).

(iv) Determine the corresponding $\alpha$ through the curve and formula in Fig. 5.

[1] L. Onsager, Phys. Rev. **37**, 405 (1931).
[2] L. Onsager, Phys. Rev. **38**, 2265 (1931).
[3] L. Onsager and S. Machlup, Phys. Rev. **91**, 1505 (1953).
[4] M. Bier and R. D. Astumian, Phys. Lett. A **247**, 385 (1998).
[5] M. Bier, I. Derényi, M. Kostur, and R. D. Astumian, Phys. Rev. E **59**, 6422 (1999).
[6] N. G. van Kampen, *Stochastic Processes in Physics and Chemistry* (Elsevier, Amsterdam, 1992).
[7] J. Klafter, M. F. Shlesinger, and G. Zumofen, Phys. Today **49**(2), 33 (1996).
[8] P. Lévy, *Calcul des Probabilités* (Gauthier-Vollars, Paris, 1925).
[9] V. M. Zolotarev, *One-Dimensional Stable Distributions* (American Mathematical Society, Providence, RI, 1986).
[10] G. Samorodnitsky and M. S. Taqqu, *Stable Non-Gaussian Random Processes* (Chapman & Hall, London, 1994).
[11] L. Chen, K. E. Bassler, J. L. McCauley, and G. H. Gunaratne, Phys. Rev. E **95**, 042141 (2017).
[12] B. Mandelbrot, J. Bus. **36**, 394 (1963).
[13] B. Mandelbrot, *The Fractal Geometry of Nature* (W. H. Freeman, San Francisco, 1983).
[14] C.-K. Peng, J. Mietus, J. M. Hausdorff, S. Havlin, H. E. Stanley, and A. L. Goldberger, Phys. Rev. Lett. **70**, 1343 (1993).
[15] M. Rypdal and K. Rypdal, Phys. Rev. Lett. **104**, 128501 (2010).
[16] P. D. Ditlevsen, Phys. Rev. E **60**, 172 (1999).
[17] K. Burnecki, A. Wyłomańska, A. Beletskii, V. Gonchar, and A. Chechkin, Phys. Rev. E **85**, 056711 (2012).
[18] K. Kanazawa, T. G. Sano, A. Cairoli, and A. Baule, Nature (Lond.) **579**, 364 (2020).
[19] J. B. Johnson, Phys. Rev. **26**, 71 (1925).
[20] Ł. Kuśmierz, A. V. Chechkin, E. Gudowska-Nowak, and M. Bier, Europhys. Lett. **114**, 60009 (2016).
[21] A. Jabłoński, Bull. l'Acad. Polon. Sci. Sér. Sci. Math., Astr. Phys. **8**, 259 (1960).
[22] See Supplemental Material at http://link.aps.org/supplemental/10.1103/PhysRevE.104.014119 for two *Mathematica* programs to generate graphs like Figs. 1(b) and 1(c).
[23] M. Bier, Phys. Rev. E **97**, 022113 (2018).
[24] K. Capała and B. Dybiec, Phys. Rev. E **102**, 052123 (2020).
[25] H. Risken, *The Fokker-Planck Equation* (Springer, Berlin, 1989).
[26] S. Jespersen, R. Metzler, and H. C. Fogedby, Phys. Rev. E **59**, 2736 (1999).
[27] M. Kateregga, S. Mataramvura, and D. Taylor, Cogent Econ. Finance **5**, 1318813 (2017).
[28] G. Muñoz-Gil *et al.*, arXiv:2105.06766.
[29] W. H. Press, B. P. Flannery, S. A. Teukolsky, and W. T. Vetterling, *Numerical Recipes in FORTRAN: The Art of Scientific Computing* (Cambridge University Press, Cambridge, UK, 1992), pp. 695–697.
[30] J. H. McCulloch, Commun. Stat.-Simul. Comput. **15**, 1109 (1986).
[31] I. A. Koutrouvelis, J. Am. Stat. Assoc. **75**, 918 (1980).
[32] A. A. Stanislavsky, K. Burnecki, M. Magdziarz, A. Weron, and K. Weron, Astrophys. J. **693**, 1877 (2009).
[33] https://www.ngdc.noaa.gov/stp/satellite/goes-r.html.
[34] L. Fletcher, B. R. Dennis, H. S. Hudson, S. Krucker, K. Phillips, A. Veronig, M. Battaglia, L. Bone, A. Caspi, Q. Chen, and P. Gallagher, Space Sci. Rev. **159**, 19 (2011).
[35] E. N. Parker, Astrophys. J. **330**, 474 (1988).
[36] E. N. Parker, Sol. Phys. **121**, 271 (1989).
[37] N. B. Crosby, M. J. Aschwanden, and B. R. Dennis, Sol. Phys. **143**, 275 (1993).
[38] S. A. Stoev, G. Michailidis, and M. S. Taqqu, IEEE Trans. Inf. Theory **57**, 1615 (2011).
[39] M. Veillette, STBL: Alpha stable distributions for MATLAB, https://github.com/markveillette/stbl.
[40] A. Seif, M. Hafezi, and C. Jarzynski, Nat. Phys. **17**, 105 (2021).
[41] É. Roldán and J. M. R. Parrondo, Phys. Rev. E **85**, 031129 (2012).
[42] U. Seifert, Rep. Prog. Phys. **75**, 126001 (2012).